A landslide velocity database for the Site C Reservoir in Northeastern British Columbia

Megan van Veen[1], Andrew Funk[2], Colleen Fish[3] & Michael Porter[2]
1. *BGC Engineering Inc., Ottawa, ON, Canada*
2. *BGC Engineering Inc., Vancouver BC, Canada*
3. *BGC Engineering Inc., Victoria, BC, Canada,*

GeoCalgary 2022 October 2-5
Reflection on Resources

ABSTRACT
The modern Peace River Valley in British Columbia contains an abundance of landslides with volumes ranging from tens of cubic metres to more than 10 million cubic metres. Landslide types in this region range from shallow slides in overburden to deep seated slides in clay shale bedrock, and often involve multi-level, complex landslide mechanisms. A landslide inventory for this region was updated by BGC in 2021 and 2022 to assign qualitative landslide behaviour types to each landslide, which reflect the dominant mode of landslide movement, long-term mean annual displacement rates, and the estimated relative frequency of faster movements. Airborne lidar change detection between 2006, 2015, 2019, and 2021 and satellite InSAR data from 2020 and 2021, coupled with select field observations, were used to estimate the velocity of landslides over each incremental date range. The velocity distributions were compared to the long-term average probability distributions (limiting state vectors) proposed for each behaviour type, which have been used to define transition matrices for Markov chain modelling of landslide velocities.

RÉSUMÉ
La vallée moderne de la rivière de la Paix en Colombie-Britannique contient une abondance de glissements de terrain avec des volumes allant de dizaines de mètres cubes à plus de 10 millions de mètres cubes. Les types de glissements de terrain dans cette région vont des glissements peu profonds dans les morts-terrains aux glissements profonds dans le substrat rocheux de schiste argileux, et impliquent souvent des mécanismes de glissement de terrain complexes à plusieurs niveaux. Un inventaire des glissements de terrain pour cette région a été mis à jour par BGC en 2021 et 2022 pour attribuer des types de comportement de glissement de terrain qualitatifs à chaque glissement de terrain, qui reflètent le mode dominant de mouvement des glissements de terrain, les taux de déplacement annuels moyens à long terme et la fréquence relative estimée des mouvements plus rapides. Les données de détection de changement de lidar aéroporté entre 2006, 2015, 2019 et 2021 ont été utilisées pour estimer la vitesse des glissements de terrain sur chaque plage de dates incrémentielle. Les distributions de vitesse ont été comparées aux modèles conceptuels de chaîne de Markov qui ont été développés pour modéliser la vitesse des glissements de terrain.

1 INTRODUCTION

The modern Peace River Valley in British Columbia contains an abundance of landslides with volumes ranging from tens of cubic metres to more than 10 million cubic metres. These landslides range from shallow slides in overburden to deep seated slides in clay shale bedrock, and often involve multi-level, complex landslide mechanisms. Numerous landslide investigations took place in the region in the 1970's, 1980's, and early 2000's forming the basis for a landslide inventory of the Site C Reservoir, which is expected to be created in 2023. This inventory was updated by BGC in 2010 and 2011 to provide interpreted mechanisms of movement for each landslide in the inventory. This analysis was primarily based on air photos, a single vintage of airborne lidar data, and field investigations, and now includes over 2000 mapped landslide complexes. In 2021 and 2022, we assigned qualitative landslide behaviour types to each landslide, which reflects the dominant mode of landslide movement, long-term mean annual displacement rates, and the estimated relative frequency of faster movements. Airborne lidar change detection between 2006, 2015, 2019, and 2021 have being used to estimate the velocity of landslides over each incremental date range, and how those velocities have changed over time. The database of landslides, landslide types, and velocities is being used to support the calibration of landslide velocity probability models and the development of precipitation and soil moisture thresholds for changes in landslide movement rates.

2 BACKGROUND

2.1 Landslide Types and Mechanisms

The geology in this area of the Peace River valley is predominantly Cretaceous sedimentary rocks (siltstone, silty shale, and sandstone) overlain by a Quaternary sequence of fluvial, glacial, and interglacial deposits, cumulatively up to 400 m thick. Post-glacial downcutting of the modern Peace River has formed steep slopes in these deposits, which are prone to landsliding. The most common expected movement types in the study area are shallow, slope parallel colluvial debris slides, rotational earth slides, and translational bedrock and earth landslides.

Many of these landslides are complex in nature, occurring along weak, near-horizontal clay layers in either the bedrock or glaciolacustrine deposits. Slides in bedrock are typically controlled by weak, pre-sheared bedding planes, sometimes bounded by relaxation joints formed during valley rebound. Slides in overburden can occur as compound soil slides (characterized by progressive movement over time) flow slides, or earth flows. In this case, we differentiate flow slides and earth flows by classifying flow-like behaviour of overburden material as a flow side, and secondary transport of either overburden or bedrock-derived colluvium as an earth flow. Example photographs of different landslide types within the study area are presented in Figure 1.

2.2 Landslide Inventory Development

In 2004, a regional landslide inventory was developed using air photos and ground-based observations (Severin, 2004). The original inventory consisted of just under 2000 mapped landslide complexes, some comprised of multiple smaller landslides with different potential failure mechanisms. In 2010 and 2011, BGC updated and expanded the original inventory, making use of airborne lidar data, collected in 2006, supplemented by 1:20,000 and 1:40,000 scale air photos and field mapping. The 2006 airborne lidar data had a bare-earth resolution of less than 1 point per square metre. The inventory refinement was conducted using the methods described in Morgan et al. (2011).

The landslides in the inventory have been mapped using a two-tiered approach: 1) landslide complexes, and 2) individual landslides within each complex. Attributes included for each individual landslide are the landslide failure mechanism, estimated basal sliding surface elevations and material types, size of each landslide (length, width, depth, and estimated volume), as well as the activity state of each sub-landslide, which was simply classified as > 100 or < 100 years old.

2.3 Landslide Velocity Models

Identifying the presence of landslides and their expected volume and failure mechanisms can provide useful information to assess the risk posed by a failure of one of these slides, however it can often be difficult to understand and predict when a change in landslide velocity may occur, specifically when a slow-moving landslide may transition to a more rapid, mobile slide. Increased landslide velocity can often be attributed to a greater level of risk, as these faster and more mobile slides can lead to greater spatial probability of impact, shorter time for avoidance (increased temporal probability), increased vulnerability, and greater economic impacts (Porter et al., 2021).

A change in the velocity of a landslide can be triggered by several factors, both natural and anthropogenic. Complex relationships are often present, which makes correlating these factors to landslide velocity difficult. Recent work by Porter et al., (2021, 2022) has proposed the use of Markov chains (Howard, 2007) for assigning probabilities to landslide velocity transitions within pre-existing slow-moving landslides. In a Markov chain model, the condition of a physical system (i.e., the landslide) can be described by state variables (e.g., the landslide velocity, or annual displacement rate). The key assumption in a Markov model is that the current state (and only the current state) can be used to determine the probability distribution of all possible condition states some number of time steps into the future. In other words, a Markov model of landslide velocity assumes that the current velocity class can be used to determine the probability distribution of the landslide moving at all possible velocity classes some number of years into the future. This probability distribution eventually converges to some long-term average distribution, referred to as the limiting state vector.

For the purpose of modelling landslide velocity probability distributions, the landslide velocity condition states have been related to the Cruden and Varnes (1996) landslide velocity classification (Table 1). In the original classification, the Very Slow velocity class corresponds to landslides with a velocity ranging from 16 mm/year to 1.6 m/year. Consistent with Porter (2021), we subdivided the Very Slow velocity class into Class 2a (> 16 mm/year) and 2b (>160 mm/year) to facilitate better characterization of the range of potential impacts from slides moving within this velocity range. The landslide velocity classes in Table 1 have been defined in terms of total annual landslide displacement criteria listed in the fourth column of the table. Further details about the proposed modified landslide velocity classification can be found in Porter et al. (2022).

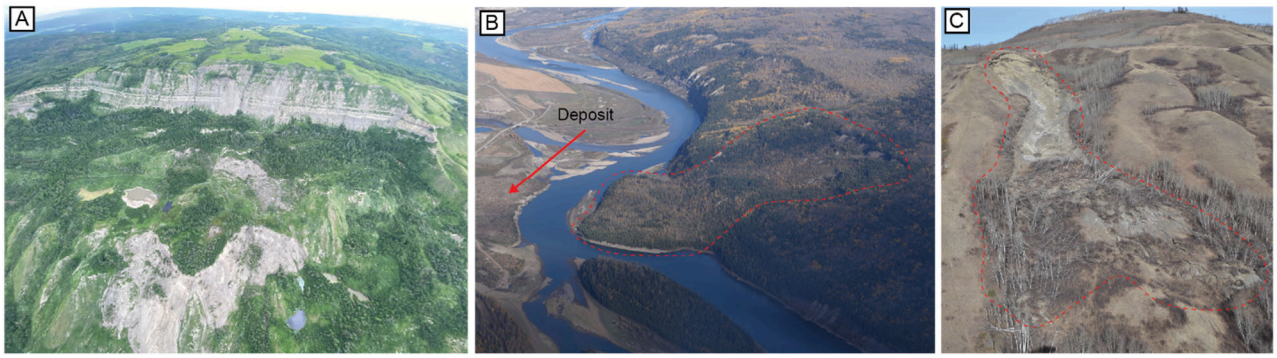

Figure 1. Landslide types within the Peace River Valley a) rock slide, b) compound earth slide and c) earth flow

Table 1. Modified landslide velocity classification after Cruden and Varnes (1996)

Class	Description	Typical velocity	Proposed annual displacement criteria (m)	Proposed mean annual displacement (m)
7	Extremely rapid	>5 m/sec		
6	Very rapid	>3 m/min		
5	Rapid	>1.8 m/hr		
4+	Moderate	>13 m/month	>16	64
3	Slow	>1.6 m/yr	>1.6	6.4
2b	Very slow	>160 mm/yr	>0.16	0.64
2a	Very slow	>16 mm/yr	>0.016	0.064
1	Extremely slow	<16 mm/yr	>0.0016	0.005
0	Dormant	0 mm/yr	<0.0016	0

Note: Class 4+ refers to all velocity classes Moderate or greater

Using a Markov chain approach, the probability of a landslide transitioning to a different velocity class or remaining in its current class is defined by a transition matrix. It is expected that different landslide types will have a different set of transition probabilities and therefore a different transition matrix. For slow-moving landslides in our study area, five different landslide behaviour types are considered, summarized in Table 2. These landslide behaviour types are intended to reflect long-term average annual displacement rates and how often more rapid movements likely occurred in the past on these slopes.

A key step in defining the transition matrices for each landslide behaviour type by Porter et al. (2022) was to assign a limiting state vector (i.e., probability distribution) that describes the long-term average distribution of landslide velocity classes for each behaviour type. These assignments were made by Porter et al. (2022) using their collective experience and judgment. Each limiting state vector can be combined with the mean annual displacement associated with each landslide velocity class to estimate the long-term average annual landslide displacement. The limiting state vector values are shown in the bottom rows of Table 2. The Site C landslide velocity database provides an opportunity to validate the assumed limiting state vectors assigned to the landslide behaviour types that are most commonly encountered in the inventory.

3 METHODOLOGY

3.1 Landslide Inventory Update

The first step in our work was to update the landslide inventory based on newer, high-resolution lidar data and lidar change detection results. Airborne lidar scanning data from 2006, 2015, 2019, and 2021 were used to perform lidar change detection across the entire study area. Change detection was performed using Iterative Closest Point (ICP) alignment techniques and 3D point-based change calculation techniques, to maximize the ability to detect slow moving landslides (van Veen et al, 2017). Any areas where ground movement was identified in the change detection results that were not previously included in the landslide inventory were added to the database. This resulted in the addition of approximately 50 landslide complexes to the inventory. The results were also used to modify the original landslide polygon boundaries. High-resolution lidar collected in 2019 and 2021 (3 to 5 points per square metre for bare-earth data) facilitated the refinement of the landslide characteristics for these new sites, as well as at existing sites where the landslides were mapped using the relatively lower resolution data from 2006 (< 1 point per square metre bare-earth data). Each landslide was assigned one of the characteristic behaviour types listed in Table 2 (Type A to Type E), based on morphological assessment of the lidar topography and the lidar change detection results.

3.2 Landslide Velocity Compilation

Landslide velocity data was compiled for a selected subset of just over 600 entries in the landslide inventory. Landslide velocities were assigned to each landslide based on the three periods of airborne lidar change detection: 2006 to 2015 (9 years), 2015 to 2019 (4 years), and 2019 to 2021 (2 years).

The airborne lidar change detection results were used to assign an average annual velocity to each landslide for the three different time periods. Satellite-based InSAR data (ALOS-2) acquired over the snow free months between spring 2020 and fall 2020 were used to refine the velocity estimates for the 2019 to 2021 period, particularly to distinguish between Velocity Class 1 and Class 2a. This analysis was completed using custom-built web-based GIS tools which allowed us to dynamically visualize the lidar change detection and InSAR monitoring results and cut slope profiles through the lidar change detection results to correlate areas of ground movement to the mapped landslide basal surfaces.

A detailed comparison between airborne lidar change detection and satellite InSAR capabilities for measuring slope displacement is summarized in van Veen et al. (2022). Typically, airborne lidar change detection can measure topographic changes on the order of 10's of cm between data acquisitions, or 8 to 10 cm between data acquisitions in the case of newer, high-resolution data. ALOS-2 InSAR is capable of measuring line of sight displacement on the order of several mm per year to 100's of mm per year, however inspection of the data for this project suggests that measurements less than 10 to 15 mm/year cannot be confidently differentiated from noise. Where no clear displacement trend could be determined from the lidar change detection or InSAR, a velocity class of 1 was assumed, so as to not overestimate the number of dormant or inactive slides in the inventory. Given the higher quality of the 2019 and 2021 airborne lidar data relative to the 2016 and 2015 data, and the ability to cross reference the InSAR monitoring results to the change detection, interpretation of the data for the 2019 to 2021 period is likely subject to fewer limitations.

Table 2. Proposed landslide behaviour types and characteristics for pre-existing slow-moving landslides (Porter et al., 2022)

Behaviour Type	Type A	Type B	Type C	Type D	Type E
Typical geology	Relatively intact shales, mudstones	Relatively intact shales, mudstones, residual soils, overconsolidated glacial deposits	Relatively intact glacial deposits, colluvium derived from shales, mudstones, residual soil and glacial deposits	Colluvium derived from shales, mudstones, residual soil and glacial deposits	Colluvium derived from shales, mudstones, residual soil and glacial deposits
Typical failure mechanism	Translational block slides and spreads	Translational block slides and spreads	Translational block slides and spreads, rotational slides, complex earth slides-earth flows	Translational slides, rotational slides, earth flows, complex earth slides-earth flows	Translational slides, rotational slides, earth flows, complex earth slides-earth flows
Typical inclination of basal shear surface	Sub-horizontal (0 to 5 degrees)	Sub-horizontal (0 to 5 degrees)	Similar to the residual friction angle	Similar to the residual friction angle	Sub-parallel to the ground surface
Typical toe condition	No toe erosion	Toe erosion usually absent	Toe erosion may be active	Toe erosion often active	Toe erosion almost always active
Long-term annual probability of Class 4+ velocities	1 in 20,000	1 in 6,500	1 in 2,000	1 in 650	1 in 200
Assumed limiting state velocity class distribution; (assumed average annual displacement for each velocity class in brackets)					
0 (0 m)	70%	50%	30%	10%	0.5%
1 (0.005 m)	28.5%	45.5%	55.0%	44.9%	3.0%
2a (0.064 m)	1.1%	3.2%	10.8%	32.4%	54%
2b (0.64 m)	0.4%	1.1%	3.6%	10.8%	36%
3 (6.4 m)	0.06%	0.18%	0.60%	1.8%	6.0%
4+ (64 m)	0.005%	0.015%	0.050%	0.15%	0.50%
Mean annual displacement	0.01 m	0.03 m	0.1 m	0.3 m	1.0 m

3.3 Velocity Transition Model Validation

Summary statistics for the compiled landslide types and velocities were generated and compared to the conceptual velocity models presented in Porter et al. (2022), for failure types that had a sufficient number of mapped landslides.

Table 3. Summary of mapped landslide types.

Type	Number of Slides	Percentage of Slides
A	6	1%
B	55	9%
C	373	61%
D	175	29%
E	2	< 1%
Total	611	

4 RESULTS

The resulting distribution of landslide types is summarized in Table 3. The distribution of landslide velocities for each of three time periods is presented in Figure 2. A general trend of increasing velocities over time is present, with fewer slides mapped as Class 0 or 1, and more slides mapped as class 2b and 3+ in the later time periods. An example is presented in Figure 3, where the lidar change detection results for each of the three time periods are shown for a Type C slide. In this example, the Velocity Class changes from Class 2a to Class 3 and then from Class 3 to Class 4 over the three comparison periods.

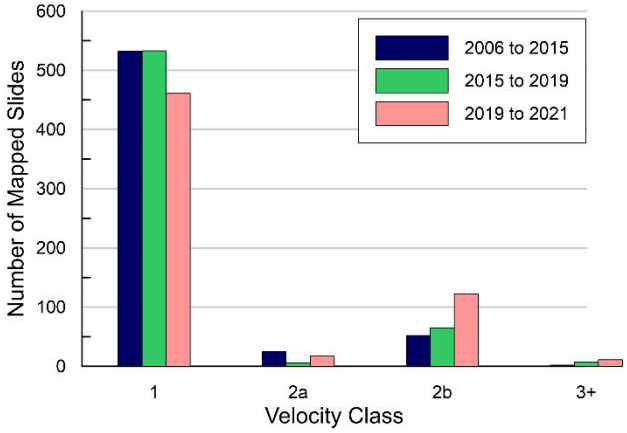

Figure 2. Distribution of velocity classes for each lidar change detection time period.

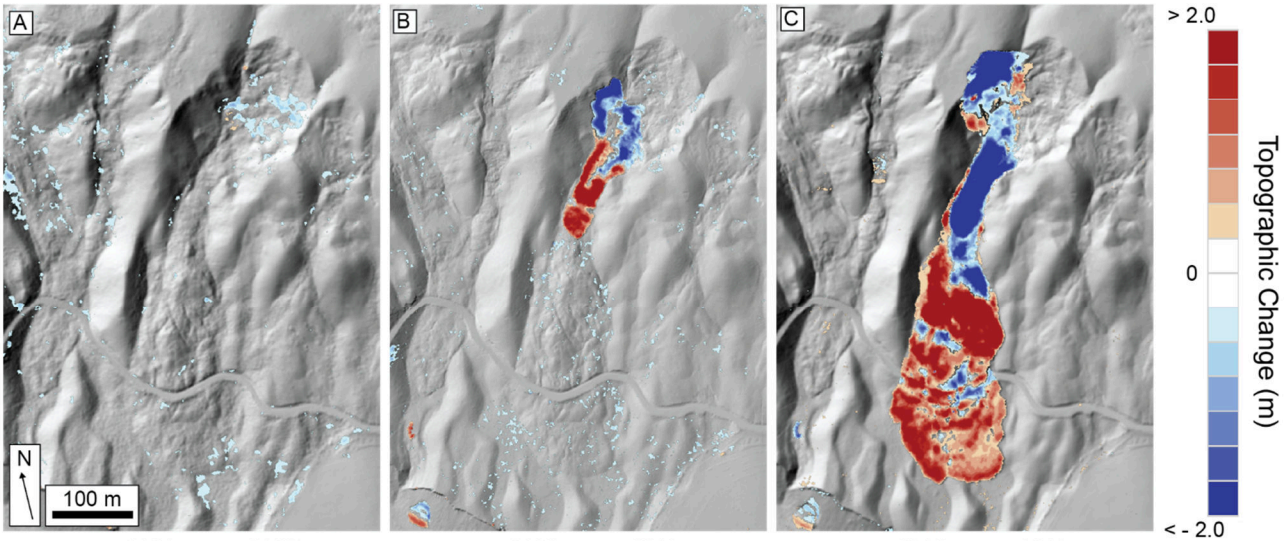

Figure 3. Airborne lidar change detection results for a Type C slide during three different time periods a) 2006 to 2015, Class 2a,

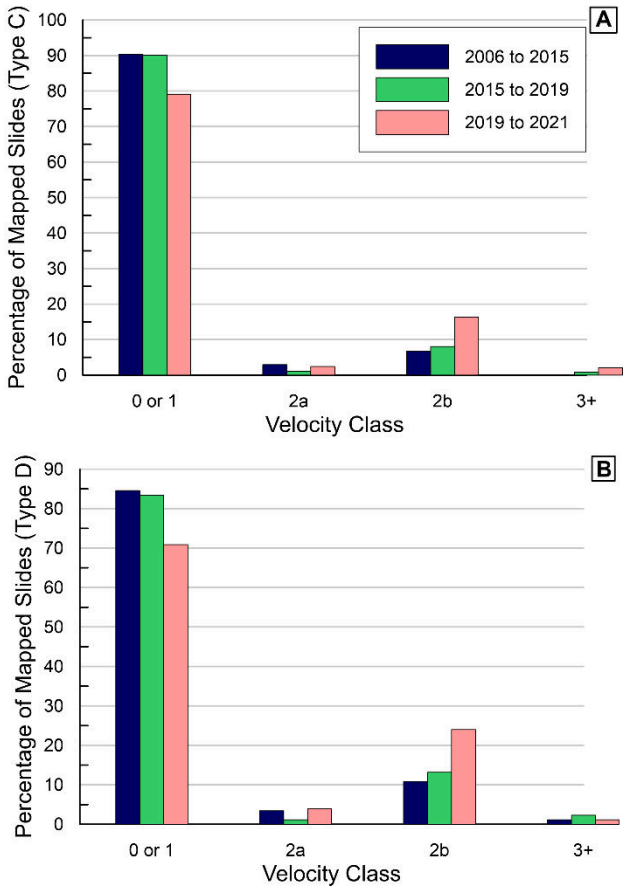

Figure 4. Comparison of velocity class distributions for a) Type C and b) Type D landslides.

The majority of mapped landslides (89%) were classified as Type C or Type D.

The velocity distributions for Type C and D slides are presented in Figure 4. These distributions are presented as a percentage of mapped slides in each type for direct comparison. A comparison to the assumed limiting state velocity distributions for each of these classes, presented in Porter et al. (2022), are provided in Table 4 and Table 5. For Type C slides, the measured landslide velocities are within 5% of the limiting state assumptions for Class 0 and 1, show a smaller percentage of slides in Class 2a and a larger percentage of slides in Class 2b, and the percentage of slides Class 3 or above is comparable to the conceptual model. For Type D slides, the percentage of slides measured to be in Velocity Class 0 and 1 or Class 2a are less than the limiting state assumptions, with the percentage of slides mapped as Class 2b 10 to 20% greater than the model, and the percentage of slides Class 3 or above comparable to the conceptual model.

Table 4. Percentage of Type C landslides in each velocity class compared to limiting state assumptions.

Velocity Class	2006 to 2015	2015 to 2019	2019 to 2021	Assumed Limiting State
0 or 1	90%	90%	79%	85.0%
2a	3%	1%	2%	10.8%
2b	7%	8%	16%	3.6%
3+	0%	< 1%	2%	< 1%

Table 5. Percentage of Type D landslides in each velocity class compared to limiting state assumptions.

Velocity Class	2006 to 2015	2015 to 2019	2019 to 2021	Assumed Limiting State
0 or 1	85%	83%	70%	95.5%
2a	3%	1%	4%	3.2%
2b	11%	13%	24%	1.1%
3+	1%	2%	1%	< 1%

5 DISCUSSION

Given that the limiting state velocity class probability distributions assigned by Porter et al. (2022) were based on judgment, it was anticipated that there would be an imperfect match with observations from the Site C landslide inventory. In many respects, the inventory observations support the judgment of Porter et al. (2022), but there are some important and unexpected differences. In particular, a relatively small proportion of slides were classified as Velocity Class 2a, and a larger proportion of slides were classified as Velocity Class 2b. Three possible reasons for this discrepancy are:

- Possible annual variations in landslide velocity classes occurring between periods of lidar acquisition;
- Limitations of the monitoring methods used to extract the velocity information; and
- Climatic conditions during the monitoring period being different than long-term average conditions.

The inability to extract more subtle temporal trends during the long period between airborne lidar scans (i.e., if a slope was moving at Class 1 or 2a for several years, but that movement is overprinted by a larger scale movement that occurred in one of the years between lidar scans).

While lidar change detection with high-quality data is capable of identifying movements greater than Velocity Class 1, it may be difficult to detect Velocity Class 2a movements unless there is a long period of time between lidar scans, allowing small movements to accumulate to a level that is above the limit of detectable change. Given that lidar change detection is measuring changes in the topographic surface, when the failure surface of a landslide is sub-parallel to the slope it is possible that the landslide can move relatively large distances, without producing detectable topographic change.

Without high-frequency data, it can be difficult to capture short to medium term temporal trends such as short-duration velocity surges. When the lidar change detection is supplemented by other monitoring tools, more detailed temporal patterns can be understood. As an example, an area with several mapped landslides on an outside river bend is presented in Figure 5. The lidar change detection results between 2019 and 2021 (Figure 5a) suggest widespread movement over this area, on the order of 2 to 3 metres over two years (upper end of Velocity Class 2b). Inspection of ALOS-2 satellite InSAR displacement results (Figure 5b) from the same time period suggest that velocities in 2020 were two to three times higher than they were in 2021 (i.e., moving at Velocity Class 2b for a year and then slowing to Velocity Class 1 or 2a, Figure 5c). In Spring 2022, a significant retrogression event on one of these slides occurred, with estimated displacement on the order of several hundred metres (Figure 5d). The timing of this event was constrained to a three-day period using freely available satellite imagery, which suggests movement within Velocity Class 5 or Velocity Class 6, that may have been averaged to a lower velocity class using lidar data collected several years apart, in the absence of other information.

Distinguishing between Velocity Class 0 and 1 without in-situ instrumentation is very much impractical, and for that reason, some assumptions must be made about when to consider a slide active or inactive based only on remote sensing monitoring. The proposed limiting state probability distributions for each landslide behaviour type provide a means of systematically assigning probabilities of Velocity Class 0 and 1 to these landslides in the absence of instrumentation data.

It is likely that the distribution of landslide velocities during any given time period will be influenced by long-term climate trends. Preliminary evidence suggests that there has been an increasing amount of precipitation in the Peace Region since approximately 2011, which may be contributing to the observed increase in faster-moving slides. Further work is underway to perform a detailed analysis of climate trends as they related to landslide displacement rates for slopes within the inventory. The availability of new tools to help characterize landslide failure mechanisms and velocity changes over time will help to improve our ability to predict future changes in velocity states.

6 CONCLUSIONS

Normally slow-moving landslides pose a risk to infrastructure, particularly during periods of faster movement. Markov chain models have been proposed to help estimate landslide velocity probability distributions which can be leveraged in landslide hazard and risk assessments. One of the key inputs to these proposed models is a limiting state probability distribution of landslide velocities for different landslide behaviour types.

Ongoing compilation of landslide velocity statistics for a large database of landslides will help to improve assumptions around the limiting state velocity class probability distributions for different landslide behaviour types in northeastern BC. The growing landslide velocity timeseries data for the Site landslide database in northeastern British Columbia will support these initiatives. There are opportunities to compile landslide velocity timeseries data from a larger group of asset owners and operators in the region, including from road, rail, and pipeline operators.

Future work will also examine correlation of changes in landslide velocity to precipitation and soil moisture trends. This will improve our ability to forecast near-term surges in landslide velocity, as well as to better anticipate changes in landslide hazard and risk associated with decadal-scale precipitation patterns and projected climate change.

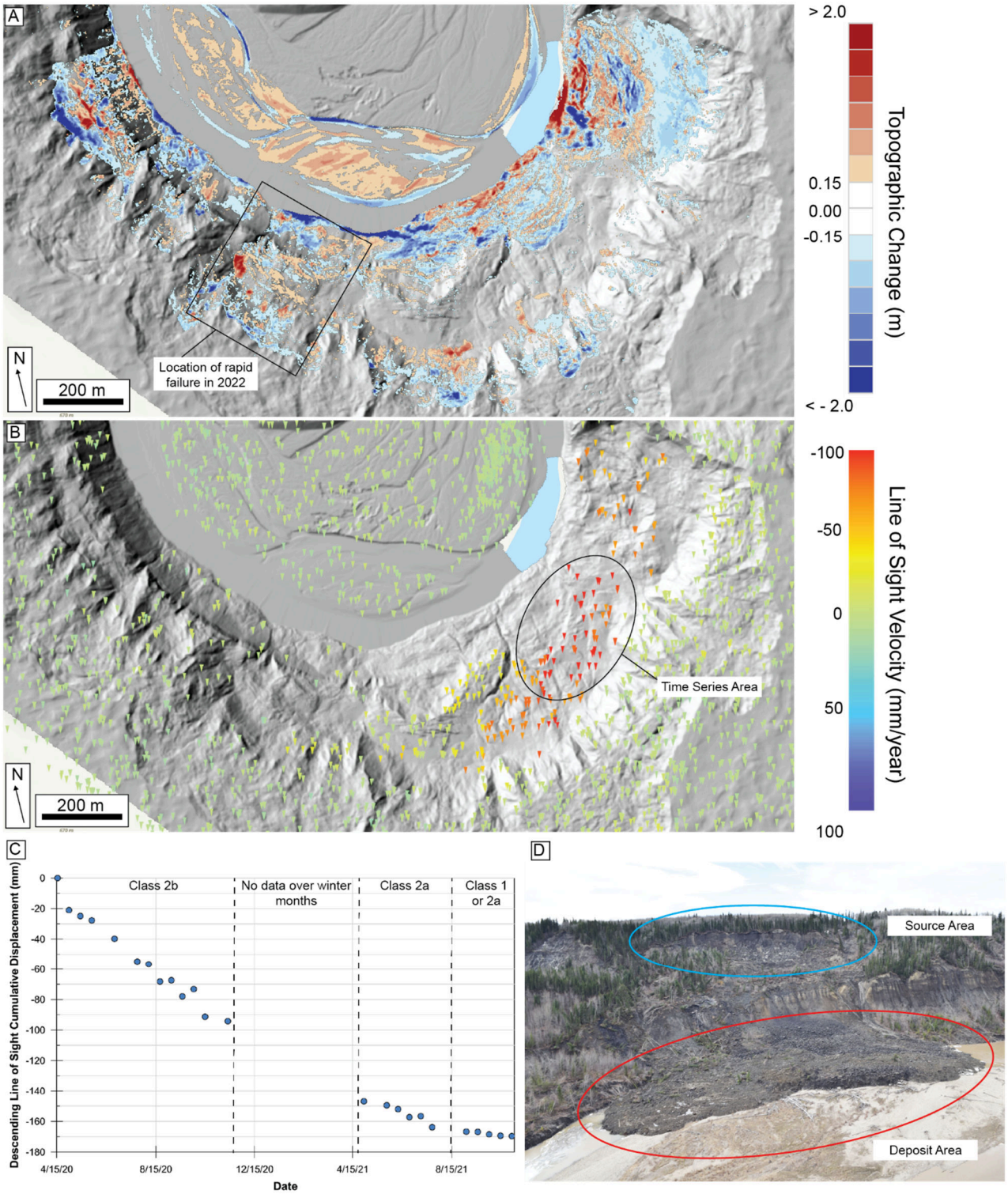

Figure 5. Example of supplementing lidar change detection results with additional information for an active area including a) airborne lidar change detection results between 2019 and 2021, b) ALOS-2 InSAR line of sight velocity measurements between 2020 and 2021, c) time-series displacements derived from InSAR measurements and d) photograph of rapid slide that occurred in Spring 2022.

7 ACKNOWLEDGEMENTS

The authors acknowledge the contributions of several of our colleagues at BGC Engineering for their support with this work, as well as the support of BC Hydro.

8 REFERENCES

Ingold, T.S. and Miller, K.S. 1983. Drained Axisymmetric Loading of Reinforced Clay, *Journal of Geotechnical Engineering*, ASCE, 109: 883-898.

Cruden, D.M. and Varnes D.J. 1996. Landslide types and processes. In: Turner and Schuster (eds) *Landslides, investigation and mitigation*, Special Report 247, Transportation Research Board, National Research Council. National Academy Press, Washington, USA, 3:36-75.

Howard, R. 2007. *Dynamic Probabilistic Systems, Volume 1: Markov Models.* Dover Publications, New York.

Morgan, A., Chao, D., Froese, C., Martin, D., and Kim, T., 2011. Lidar based landslide inventory and spatial analysis, Peace River Alberta, *Geohazards 5*, 5th Canadian Geohazards Conference, Kelowna, BC, Canada.

Porter, M. 2021. Conceptual Markov models for estimating velocity transition probabilities for landslides in the Western Canadian Sedimentary Basin, *GeoNiagara*, Canadian Geotechnical Conference, Niagara Falls, ON, Canada.

Porter, M., Quinn, P., and Barlow, P. 2022. Conceptual landslide velocity transition models for a range of landslide behaviour types, *Geohazards 8*, 8th Canadian Geohazards Conference, Quebec City, QC, Canada.

Severin, J. 2004. Landslides in the Charlie Lake Map Sheet, Fort St. John. M.A.Sc. Thesis. The University of British Columbia.

van Veen, M., Lato, M., van Hove, J., Hunchuk, G., Babcock, J., and Bracic, J. 2017. The use of airborne lidar in understanding ground hazards for large pipeline networks, *GeoOttawa*, Canadian Geotechnical Conference, Ottawa, ON, Canada.

Van Veen, M., Lato, M., Mitchell, A., Froese, C., and Porter, M. 2022. Practical considerations for monitoring landslides on critical slopes. *Geohazards 8*. Quebec City, QC, Canada.